



1 **Oxygen isotope composition of waters recorded in carbonates in strong clumped and oxygen**
2 **isotopic disequilibrium**

3

4 **Caroline Thaler^{1*}, Amandine Katz¹, Magali Bonifacie¹, Bénédicte Ménez¹, Magali Ader¹**

5 ¹ Université de Paris, Institut de physique du globe de Paris, CNRS, F-75005 Paris France

6 ***corresponding author: Thaler.caroline@gmail.com**

7

8 **Abstract.** Paleoenvironmental reconstructions, which are mainly retrieved from oxygen isotope ($\delta^{18}\text{O}$)
9 and clumped isotope (Δ_{47}) compositions of carbonate minerals, are compromised when carbonate
10 crystallization occurs in isotopic disequilibrium. To date, knowledge of these common isotopic
11 disequilibria, known as vital effects in biogenic carbonates, remains limited and the potential
12 information recorded by $\delta^{18}\text{O}$ and Δ_{47} offsets from isotopic equilibrium values is largely overlooked.
13 Additionally, in carbonates formed in isotopic equilibrium, the use of the carbonate $\delta^{18}\text{O}$ signature as a
14 paleothermometer relies on our knowledge of the paleowaters' $\delta^{18}\text{O}$ value, which is often assumed.
15 Here, we report the largest Δ_{47} offsets observed to date (as much as -0.270‰), measured on microbial
16 carbonates, that are strongly linked to carbonate $\delta^{18}\text{O}$ offsets (-25‰) from equilibrium. These offsets are
17 likely both related to the microorganism metabolic activity and yield identical erroneous temperature
18 reconstructions. Unexpectedly, we show that the $\delta^{18}\text{O}$ value of the water in which carbonates
19 precipitated, as well as the water-carbonate $\delta^{18}\text{O}$ fractionation dependence to temperature at equilibrium
20 can be retrieved from these paired $\delta^{18}\text{O}$ and Δ_{47} disequilibrium values measured in carbonates. The
21 possibility to retrieve the $\delta^{18}\text{O}$ value of paleowaters, sediments' interstitial waters or organisms' body
22 water at the carbonate precipitation loci, even from carbonates formed in isotopic disequilibrium, opens



23 long-awaited research avenues for both paleoenvironmental reconstructions and biomineralization
24 studies.

25

26 **1 Introduction**

27 Oxygen isotope composition ($\delta^{18}\text{O}$) paired with clumped isotope composition (Δ_{47}) of carbonate
28 minerals is increasingly used for reconstructing paleoenvironmental or diagenetic conditions (Ghosh et
29 al., 2006; Mangenot et al., 2017; Henkes et al., 2018). The $\delta^{18}\text{O}$ composition of carbonates depends on
30 both the $\delta^{18}\text{O}$ value of the water in which the carbonate precipitated and the precipitation temperature
31 (Urey et al., 1951). Its use to reconstruct paleoenvironments can be combined with the new carbonate C-
32 O “clumped isotopes” abundancy (Δ_{47}) thermometer which depends only on the carbonate precipitation
33 temperature (Ghosh et al., 2006). By combining the Δ_{47} derived temperatures and the carbonate $\delta^{18}\text{O}$
34 value ($\delta^{18}\text{O}_{\text{carbonate}}$), the $\delta^{18}\text{O}$ value of the water ($\delta^{18}\text{O}_{\text{water}}$) in which the carbonate precipitated can be
35 retrieved. However, this requires that solid carbonate and water reached isotopic equilibrium, which is
36 often hard to prove. Conversely, carbonate precipitation in isotopic disequilibrium is commonly
37 encountered (Affek et al., 2014; Loyd et al., 2016). Out of equilibrium $\delta^{18}\text{O}$ and Δ_{47} values are
38 particularly known to occur in biogenic carbonates (Thiagarajan et al., 2011, Bajnai et al., 2018)—the
39 most abundant carbonates in the sedimentary record. To date, the reasons for these isotopic disequilibria
40 in carbonates remain largely under-constrained. While Δ_{47} compositions of carbonates seemed at first
41 free of any biologically-driven or mineral-specific fractionation known to affect $\delta^{18}\text{O}_{\text{carbonate}}$
42 compositions (Eiler, 2011), recently identified disequilibrium Δ_{47} values (Saenger et al., 2012; Affek,
43 2013; Tang et al., 2014; Burgener et al., 2018) open new perspectives to unravel the mechanisms
44 responsible for oxygen isotopic disequilibrium in carbonate minerals. More specifically, it has become
45 crucial to determine if the $\delta^{18}\text{O}$ and Δ_{47} disequilibria observed in carbonates as diverse as those found in



46 coral reefs (Saenger et al., 2012), brachiopods (Bajnai et al., 2018), microbialites and methane seep
47 carbonates (Loyd et al., 2016), along with speleothems (Affek et al., 2014) could be explained by
48 oxygen-isotope disequilibria occurring in dissolved inorganic carbon (DIC) involved in carbonate
49 precipitation. In this case, $\delta^{18}\text{O}$ and Δ_{47} disequilibria in biogenic carbonates would record information,
50 however unavailable yet, on the physiological characteristics of carbonate-forming organisms.

51 In previous experiments we produced microbial calcium carbonates (Millo et al., 2012; Thaler et
52 al., 2017) that recorded the strongest oxygen isotope disequilibrium ever identified between DIC and
53 precipitation water (*i.e.* -25‰ offset from $\delta^{18}\text{O}_{\text{carbonate}}$ equilibrium values). We used carbonic anhydrase
54 (CA), an enzyme able to accelerate oxygen isotope equilibration between DIC and water *via* fast CO_2
55 hydration and HCO_3^- dehydration. When CA was added to the precipitation water, the carbonate oxygen
56 isotope compositions reached equilibrium with the precipitation water (Thaler et al., 2017). Here, we
57 build up on these experiments as they offer a unique opportunity to assess experimentally whether
58 carbonates precipitated from DIC in disequilibrium with water also record Δ_{47} disequilibrium values, and
59 the type of information that is actually carried by these paired disequilibria. We latter show how and to
60 what extent this can be applied to previously published cases of oxygen isotopic offsets from
61 equilibrium values in both biogenic and abiotic carbonates.

62

63 **2 Material and Methods**

64 **2.1 Precipitation of microbial carbonates**

65 Carbonates were precipitated at $30 \pm 0.1^\circ\text{C}$ using the procedure detailed in Millo et al., (2012) and Thaler
66 et al., (2017) and summarized hereafter. The precipitation solution (initial pH = 6.0) was composed of
67 ions added to Milli-Q[®] water (resistivity = $18 \text{ M}\Omega\cdot\text{cm}$) by dissolving salts in the following order:
68 $\text{MgSO}_4\cdot 7\text{H}_2\text{O}$ (16 mM), NaCl (80 mM), KCl (4 mM), urea (33.3 mM), CaCl_2 (40 mM). The aim was to



69 mimic the ionic composition of a groundwater (Millo et al., 2012). In experiments with CA whose $\delta^{18}\text{O}$
70 results (but not the Δ_{47} ones) were recently published in Thaler et al., (2017), the precipitation solution
71 was supplemented with CA at a concentration of 2 mg/L. The precipitation solution (with or without
72 CA) was then mixed at a volumetric ratio of 1:1 with the ureolytic soil bacteria *Sporosarcina pasteurii*
73 suspended in Milli-Q[®] water, at a final optical density at 600 nm of 0.100 ± 0.010 . For this study, 16
74 gastight Exetainer[®] vials were filled with the precipitation solution without CA in order to sacrifice them
75 at regular time intervals (*i.e.* 30, 60, 120, 180, 360 min and 24 h) and thus obtain information on the
76 kinetics of the reaction, while reproducing the procedure followed for the experiment with CA (Thaler et
77 al., 2017) consisting of 27 vials sacrificed every 10 to 30 min and after 24 h. The vials capped with
78 rubber septa were filled up to the brim, *i.e.* without headspace, hence preventing any gaseous exchange
79 with the atmosphere or headspace gases. Ureolysis completion was followed by evaluating the
80 production of dissolved inorganic nitrogen ($\text{DIN} = \text{NH}_3 + \text{NH}_4^+$). Determination of pH, DIN concentration
81 and amount of precipitated carbonates (Supplementary Fig. 2), as well as isotopic measurements, were
82 performed for each vial to monitor their evolution as the ureolysis reaction progresses. The pH initially
83 increased from 6.0 to 9.0 due to NH_3 production by ureolysis and consecutive alkalization of the
84 precipitation solution (Supplementary Fig. 2a). The subsequent carbonate precipitation (Supplementary
85 Fig. 2b) lowered pH to 8.6 (without CA) and 8.5 (with CA) and was followed by a second pH increase
86 to 8.8 (without CA) and 8.7 (with CA) when carbonate precipitation stopped while ureolysis continued.
87 At ureolysis completion, all the calcium initially present in solution (*i.e.* the limiting reagent) has
88 precipitated whereas 35 to 45% of the DIC produced by ureolysis remained in solution. Carbonate
89 precipitates, formed at the bottom and on the wall of the vials, were immediately rinsed with a few drops
90 of pure ethanol in order to dehydrate bacteria and prevent further ureolysis, carbonate formation and/or
91 dissolution–reprecipitation processes. Ethanol was then removed, and prior to their collection,



92 carbonates were dried overnight at 40°C in the vials placed in a ventilated oven equipped with
93 desiccating beads. All of the measured chemical parameters (pH, DIC, amount of solid carbonates, Ca²⁺
94 concentration, DIN) along with DIC and solid carbonate $\delta^{13}\text{C}$ behave similarly with or without active
95 CA (Thaler et al., 2017). It was not possible to measure Δ_{47} for all the precipitated carbonates due to
96 their low amount, particularly for the tubes sacrificed at the beginning of the experiments
97 (Supplementary Table 1).

98

99 **2.2 $\delta^{18}\text{O}$ and Δ_{47} measurements and associated uncertainties**

100 All the isotopic analyses were made at Institut de physique du globe de Paris (IPGP, France). $\delta^{18}\text{O}$
101 analyses were performed on carbonate powders of ca. 2 mg with a continuous helium-flow isotope ratio
102 mass spectrometer AP 2003 (Analytical Precision 2003, GV Instruments) coupled to a gas
103 chromatograph column (GC-IRMS, Chrompac Column Type 99960), as described in Millo et al., (2012)
104 and Thaler et al., (2017). External reproducibility on carbonate standards is $\pm 0.1\text{‰}$ (1SD) and represents
105 the uncertainty assigned to $\delta^{18}\text{O}_{\text{carbonate}}$ data.

106 The analytical procedure used for clumped isotope Δ_{47} measurements is only briefly presented
107 here and detailed in Bonifacie et al., (2017). About 5 mg of carbonates were digested at 90°C during 20
108 min with 104% phosphoric acid H_3PO_4 in a common acid bath. The produced gaseous CO_2 was purified
109 with a manual vacuum line before introduction into a Thermo Scientific MAT 253 dual-inlet mass
110 spectrometer. Each purified CO_2 gas was analyzed for their abundance in isotopologues with m/z from
111 44 to 49 versus a working gas provided by Oztech Trading Corporation with $\delta^{13}\text{C} = -3.71\text{‰}$ VPDB and
112 $\delta^{18}\text{O} = +24.67\text{‰}$ VSMOW, as determined with the international reference material NBS19. One single
113 Δ_{47} measurement corresponds to 70 cycles of 26 s integration time each (total integration time = 1820 s).
114 Conventional $\delta^{18}\text{O}$ and $\delta^{13}\text{C}$ data were also acquired simultaneously to Δ_{47} measurements with this



115 instrument (Supplementary Tables 1 and 3). They are in excellent consistency with data obtained with
116 the continuous-flow method on smaller samples (Supplementary Table 1).

117 The Δ_{47} is calculated as a function of the stochastic distribution of the CO₂ isotopologues, as
118 follows:

$$119 \quad \Delta_{47} = \left[\left(\frac{R_{measured}^{47}}{R_{stochastic}^{47}} - 1 \right) - \left(\frac{R_{measured}^{46}}{R_{stochastic}^{46}} - 1 \right) - \left(\frac{R_{measured}^{45}}{R_{stochastic}^{45}} - 1 \right) \right] \times 1000 \quad (1),$$

120 where Δ_{47} is expressed in per mil (‰), and R^{47} , R^{46} and R^{45} are the abundance ratios of the masses 47,
121 46, 45 respectively, relative to the mass 44 (¹²C¹⁶O¹⁶O). $R_{measured}^X$ are measured ratios inside the CO₂
122 sample. $R_{stochastic}^X$ are calculated from the measured 44, 45, 46 and 47 abundance ratios. The amount of
123 isotopologues of mass 47 (mainly ¹³C¹⁸O¹⁶O, but also ¹²C¹⁷O¹⁶O and ¹³C¹⁷O¹⁷O) measured within the
124 CO₂ sample extracted from the acid digestion of the carbonates is linked to the amount of isotopologues
125 of mass 63 (mainly ¹³C¹⁸O¹⁶O¹⁶O) within the reacted carbonate mineral (Guo et al., 2009). For the
126 correction from ¹⁷O interferences we used the ¹⁷O correction parameters from Brand et al., (2010), as
127 recently recommended (Daëron et al., 2016). In order to transfer the obtained raw Δ_{47} data into the
128 absolute Carbon Dioxide Equilibrated Scale “CDES” (Δ_{47}^{CDES90} being the Δ_{47} values of carbonates
129 reacted within acid at 90°C), standards of CO₂ gases equilibrated at 25°C and 1000°C and with bulk
130 isotopic compositions covering the range of measured carbonate samples (δ^{47} values between -50 and
131 +24‰) were analyzed interspaced with unknown samples (typically 15 equilibrated CO₂ gas analyses by
132 discrete session of analysis, 4 analytical sessions in total; Supplementary Table 4). For each analytical
133 session, as recommended in Dennis et al., (2011), the Δ_{47} data were finally corrected with a fixed
134 Equilibrated Gas Line slope (only slightly varying from 0.0048 to 0.0062 over our analytical sessions)
135 and an Empirical Transfer Function (slopes varying from 1.0859 to 1.1344) based on the equilibrated
136 CO₂ standards. Finally, the accuracy of our whole dataset and processing procedure was validated on
137 carbonate reference material (*i.e.* IPGP-Carrara and 102-GC-AZ01), typically analyzed every 2



138 unknown samples (Supplementary Table 4). The Δ_{47} values obtained at IPGP over the course of this
139 study are $\Delta_{47}^{\text{CDES90}} = 0.316 \pm 0.020\text{‰}$ (1SD, $n = 16$) for IPGP-Carrara and $\Delta_{47}^{\text{CDES90}} = 0.620 \pm 0.010\text{‰}$
140 (1SD, $n = 18$) for 102-GC-AZ01. Those values are indistinguishable from the values obtained at IPGP
141 over four years of analyses on the same instrument ($n > 300$) or previously reported by other laboratories
142 (Daëron et al., 2016).

143

144 2.3 Temperature estimates and associated uncertainties

145 Apparent temperatures issued from oxygen isotope compositions were calculated based on the measured
146 $\delta^{18}\text{O}_{\text{carbonate}}$ values of both the precipitated carbonate and the precipitation water in each experimental
147 vial (Supplementary Table 1) and using the equation of oxygen isotopes' fractionation between calcite
148 and water from Kim and O'Neil, (1997). Apparent temperatures issued from clumped isotope
149 compositions were calculated from $\Delta_{47}^{\text{CDES90}}$ data using the composite universal Δ_{47} -T calibration (Eq. 3
150 from Bonifacie et al., (2017) with T, the temperature). It is noteworthy that our main observations and
151 conclusions do not change if other calibrations to temperature are used for $\delta^{18}\text{O}$ and/or Δ_{47} (Kelson et al.,
152 2017) (see also Supplementary Discussion and Supplementary Table 2). For both proxies, the reported
153 uncertainties on temperature estimates correspond to the standard deviation of the mean of replicated
154 isotopic measurements of the same powder propagated in the calibration equation (but the actual errors
155 on the calibration themselves are not considered). Note that the long-term external reproducibility on
156 homogeneous calcite reference materials found in this study (*i.e.* $\pm 0.020\text{‰}$, 1SD) is used for samples
157 with only one measurement or with 1SD lower than 0.020‰ (Supplementary Tables 1 and 4,
158 Supplementary Discussion).

159

160 3 Results and Discussion



161 **3.1 Δ_{47} and $\delta^{18}\text{O}$ compositions of microbial carbonates can present strongly correlated vital**
162 **effects**

163 We performed Δ_{47} measurements on (i) microbial carbonates precipitated without CA by faithfully
164 replicating the experiment detailed in Thaler et al., (2017) and (ii) microbial carbonates precipitated in
165 the presence of CA remaining from these experiments. These calcium carbonates were precipitated as
166 the result of microbially-driven hydrolysis of urea into DIC and ammonia (Millo et al., 2012). They
167 constitute a reliable model for carbonate precipitation triggered by enzymatic production or transport of
168 DIC, as it is the case for micro- and macro-skeletal carbonates common in the Phanerozoic, and for
169 microbially-mediated carbonates since the Precambrian.

170 Without CA, the isotopic values of the very first carbonate precipitates present strong isotopic offsets
171 from equilibrium values, down to -0.270‰ for Δ_{47} (the largest Δ_{47} offset ever measured in solid
172 carbonates) and -24.7‰ for $\delta^{18}\text{O}_{\text{carbonate}}$ (Fig. 1 and Supplementary Table 1). Both Δ_{47} and $\delta^{18}\text{O}_{\text{carbonate}}$
173 absolute values then increase as ureolysis progresses, reducing offsets from equilibrium values to -
174 0.179‰ for Δ_{47} and -15.7‰ for $\delta^{18}\text{O}_{\text{carbonate}}$. In the presence of CA, the trends observed for the Δ_{47} and
175 $\delta^{18}\text{O}_{\text{carbonate}}$ values are similar but the offsets from equilibrium are drastically reduced (down to -0.027‰
176 for Δ_{47} and -1.4‰ for $\delta^{18}\text{O}_{\text{carbonate}}$ at the end of the experiment; Fig. 1), hence attesting for on-going
177 isotopic equilibration of DIC with water by CA enzymatic activity prior to and during carbonate
178 precipitation. The comparable behavior of Δ_{47} and $\delta^{18}\text{O}_{\text{carbonate}}$ values with respect to CA suggests that
179 both disequilibria are inherited from the $\delta^{18}\text{O}$ and Δ_{47} signatures of the DIC generated by the biological
180 activity.

181

182 **3.2 Δ_{47} and $\delta^{18}\text{O}_{\text{carbonate}}$ disequilibrium originate from the metabolic production of DIC**



183 Here, we discuss the potential processes known to generate $\delta^{18}\text{O}$ and Δ_{47} isotope fractionations during
184 carbonate precipitation and we identify the main mechanism explaining our paired Δ_{47} and $\delta^{18}\text{O}_{\text{carbonate}}$
185 disequilibria. The relatively high precipitation rate (R) in our experiments ($\log R = -3.95 \text{ mol} \cdot \text{m}^{-2} \cdot \text{s}^{-1}$;
186 (Thaler et al., 2017)) can only account for an oxygen kinetic isotope fractionation (KIF) of about 1 to
187 2‰ for $\delta^{18}\text{O}$ values (Watkins et al., 2013), while the oxygen isotope disequilibrium recorded in our
188 carbonates reaches -24.7‰. Degassing of CO_2 , known to fractionate DIC oxygen isotopes (Affek and
189 Zaarur, 2014), can be ruled out as there is no gas phase in our experiments (see Material and Methods).
190 Any potential kinetic fractionation due to DIC diffusion (Thiagarajan et al., 2011) is also unlikely as
191 precipitation occurred on the bacterial DIC-producing cells, as highlighted by scanning electron
192 microscopy showing bacterial cells trapped within and at the surface of carbonate crystals
193 (Supplementary Fig. 1). Accordingly, the large offsets from equilibrium values observed for both Δ_{47}
194 and $\delta^{18}\text{O}$ in our microbial carbonates can only result from (i) a KIF induced by CO_2
195 hydration/hydroxylation into HCO_3^- (but only if ureolysis produces CO_2 rather than H_2CO_3 , which has
196 not been established yet (Matsuzaki et al., 2013)) or (ii) a metabolic isotopic signature of the DIC
197 produced by the bacteria, inherited from the initial isotopic composition of urea and/or due to a KIF
198 introduced by the urease enzyme. CO_2 hydration/hydroxylation leads to the formation of HCO_3^- , with
199 two oxygen atoms coming from CO_2 and the third one from H_2O (hydration) or OH^- (hydroxylation).
200 The $\delta^{18}\text{O}_{\text{HCO}_3^-}$ value can then be estimated using a simple mass balance calculation (Létolle et al., 1990b;
201 Usdowski et al., 1991). The newly formed HCO_3^- is enriched in ^{16}O compared to the reacting CO_2
202 because of the incorporation of oxygen coming from H_2O or OH^- , both enriched in ^{16}O relative to ^{18}O in
203 contrast with CO_2 (Green and Taube, 1963; Beck et al., 2005). Such a low $\delta^{18}\text{O}_{\text{HCO}_3^-}$ value, several per
204 mil lower than the equilibrium one, can then be preserved in the calcium carbonate if precipitation
205 occurs shortly after CO_2 hydration/hydroxylation and before the full equilibration with water (Rollion-



206 Bard et al., 2003). Regarding clumped isotopes, ab initio calculations predict that the fractionation
207 associated with CO₂ hydration/hydroxylation increases the relative abundance of ¹³C-¹⁸O bonds, and
208 thus the Δ₄₇ value (Guo, Ms 2009). Even though this predicted fractionation trend has previously been
209 used to explain several datasets for which CO₂ hydroxylation was assumed to occur prior to carbonate
210 precipitation (Tripathi et al., 2015; Spooner et al., 2016), such a tendency can only be validated using data
211 acquired on carbonates for which CO₂ hydration/hydroxylation is demonstrated. This is the case of (i)
212 hyperalkaline travertines (Falk et al., 2016) even though part of the reported kinetic isotope fractionation
213 can be interpreted as resulting from CO₂ dissolution process (Clark et al., 1992) and (ii) two
214 experimental samples (Tang et al., 2014) precipitated at high pH where CO₂ hydroxylation dominates.
215 Both studies show, in agreement with the ab initio calculations (Guo, Ms 2009), higher Δ₄₇ and lower
216 δ¹⁸O_{carbonate} values compared to equilibrium. Thus, in a case where ureolysis would produce CO₂ in
217 isotopic equilibrium with water, the Δ₄₇ values affected by CO₂ hydration/hydroxylation recorded in
218 calcium carbonates should be higher than the equilibrium value, while our microbial carbonates are
219 showing Δ₄₇ values lower than equilibrium. Thus, we conclude that our low Δ₄₇ values measured in
220 carbonates can only be explained by a metabolic source effect. In our case it corresponds to the ureolytic
221 production of DIC, either directly as H₂CO₃ or as CO₂, with a Δ₄₇ value low enough to compensate for
222 any potentially succeeding increase due to the KIF associated with CO₂ hydration/hydroxylation.
223 Nonetheless, the slow but continuous increase observed in our experiment without CA for both Δ₄₇ and
224 δ¹⁸O_{carbonate} values more likely reflects ongoing equilibration of DIC oxygen isotopes with water at a
225 slow rate.

226 Our results highlight that the isotope clumping proceeds continuously as C-O bonds are breaking
227 and re-forming in the DIC, allowing oxygen isotopes (¹⁶O, ¹⁷O and ¹⁸O) to be redistributed between
228 H₂O, OH⁻, H₂CO₃, HCO₃⁻ and CO₃²⁻ species *via* H₂O/OH⁻ -attachment to CO₂ and -detachment from



229 HCO_3^- . In the experiment with CA, both Δ_{47} and $\delta^{18}\text{O}_{\text{carbonate}}$ reach simultaneously values close to
230 equilibrium and without CA both Δ_{47} and $\delta^{18}\text{O}_{\text{carbonate}}$ values increase simultaneously. This coevolution
231 corroborates former observations of comparable kinetics for clumped isotopes and $\delta^{18}\text{O}$ equilibration
232 between DIC and water or CO_2 and water once $\delta^{13}\text{C}$ is equilibrated (Affek, 2013; Clog et al., 2015). This
233 principle has been used to correct for disequilibrium fractionation factor in speleothems (Affek et al.,
234 2008).

235

236 **3.3 Erroneous yet comparable temperatures reconstructed from disequilibrium Δ_{47} and $\delta^{18}\text{O}$** 237 **values in carbonates**

238 Apparent temperatures were calculated from disequilibrium Δ_{47} values obtained in the experiment
239 without CA using calibration of Bonifacie et al., (2017). Ranging from $198 \pm 21^\circ\text{C}$ to $115 \pm 8^\circ\text{C}$ (Fig. 2),
240 they are at odds with the actual precipitation temperature of $30 \pm 1^\circ\text{C}$ (see Methods). This shows that
241 when carbonates precipitate from DIC in oxygen-isotope disequilibrium with water, the abundance of
242 ^{13}C - ^{18}O bonds in carbonates does not correlate with precipitation water temperature. Conversely, the
243 temperatures reconstructed from the Δ_{47} values of carbonates precipitated in the presence of CA, ranging
244 from $47 \pm 6^\circ\text{C}$ to $39 \pm 2^\circ\text{C}$, are much closer to the actual precipitation temperature. Interestingly, the
245 apparent temperatures reconstructed using Kim and O'Neil et al., (1997) calibration from the $\delta^{18}\text{O}_{\text{carbonate}}$
246 and $\delta^{18}\text{O}_{\text{water}}$ values of the same samples show comparable offsets from the actual temperature in both
247 experiments without CA (from $218 \pm 2^\circ\text{C}$ to $139 \pm 1^\circ\text{C}$) and with CA (from $39 \pm 1^\circ\text{C}$ to $37 \pm 1^\circ\text{C}$) (Fig. 2).
248 Practically, this implies that similar temperatures calculated from both carbonate Δ_{47} and $\delta^{18}\text{O}_{\text{carbonate}}$
249 values (in a case where the precipitation water $\delta^{18}\text{O}$ can be determined) can neither constitute evidence
250 against O-isotope disequilibrium nor confirm that this is the true precipitation temperature.

251



252 **3.4 Δ_{47} and $\delta^{18}\text{O}_{\text{carbonate}}$ paired disequilibria record the $\delta^{18}\text{O}$ of the water in which the**
253 **carbonates precipitated**

254 The fact that both Δ_{47} and $\delta^{18}\text{O}_{\text{carbonate}}$ values permit to calculate similarly evolving apparent
255 temperatures along the (dis)equilibration profile recorded in carbonates as the experiment proceeds,
256 indicates that the $\delta^{18}\text{O}_{\text{carbonate}}$, $\delta^{18}\text{O}_{\text{water}}$, Δ_{47} , and apparent temperature values are all together linked. In a
257 Δ_{47} versus $\delta^{18}\text{O}_{\text{carbonate}}$ diagram, all of our data align, irrespectively of the fact that they are in strong
258 isotopic disequilibrium or close to equilibrium (Fig. 3). Their alignment is fitted with what would be
259 expected for equilibrium Δ_{47} and $\delta^{18}\text{O}_{\text{carbonate}}$ values of calcite precipitated at various temperatures from a
260 water at a given $\delta^{18}\text{O}_{\text{water}}$ value. This $\delta^{18}\text{O}_{\text{water}}$ value can be calculated by combining for the same
261 temperature, the equations of Δ_{47} and $\delta^{18}\text{O}_{\text{carbonate}}$ temperature calibrations from Kim and O'Neil, (1997)
262 and Bonifacie et al., (2017), respectively (Eq. 2):

$$263 \quad \delta^{18}\text{O}_{\text{water}} = \exp \left[- \frac{18.03}{\sqrt{\frac{0.0422 \times 10^6}{\Delta_{47} \text{ CDES90}^{-0.1126}}}} + 32.42 \times 10^{-3} + \ln(\delta^{18}\text{O}_{\text{carbonate}} + 1000) \right] - 1000 \quad (2),$$

264 with $\delta^{18}\text{O}_{\text{water}}$ and $\delta^{18}\text{O}_{\text{carbonate}}$ values in the same isotopic referential (here VSMOW), and Δ_{47} values
265 reported into the absolute Carbon Dioxide Equilibrated Scale ($\Delta_{47} \text{ CDES90}$). The calibration of Kim and
266 O'Neil, (1997) was preferred over more recent calibration equations (e.g. Watkins et al., 2013) because
267 it provides the best consistency for temperatures reconstructed from both the carbonate $\delta^{18}\text{O}$ and Δ_{47}
268 values at temperatures above 100°C. Note that Kim and O'Neil, (1997) and Bonifacie et al., (2017)
269 calibrations were developed independently, which prevents circular reasoning. Finally, as Kim and
270 O'Neil, (1997) is the most used calcite calibration to date, it also allows for a broader comparison with
271 previously published results.

272 Despite the fact that the data present a large range of offsets from equilibrium (Fig. 3), the mean
273 $\delta^{18}\text{O}_{\text{water}}$ value calculated using Eq. 2 for each combination of Δ_{47} and $\delta^{18}\text{O}_{\text{carbonate}}$ values measured for
274 our carbonates is $-8.0 \pm 2.8\%$ (1SD), indistinguishable (*i.e.* within errors) from the $\delta^{18}\text{O}_{\text{water}}$ values



275 measured in our experiments ($-6.4 \pm 0.2\%$ with CA and $-6.8 \pm 0.2\%$ without CA; Fig. 3). Note that such
276 precision in $\delta^{18}\text{O}_{\text{water}}$ values found in disequilibrium carbonates is remarkable considering that even for
277 equilibrium carbonates, $\delta^{18}\text{O}_{\text{water}}$ can only be retrieved from paired Δ_{47} and $\delta^{18}\text{O}_{\text{carbonate}}$ values with a
278 precision of $\pm 1\%$ at best (see Supplementary information). This opens the promising opportunity to
279 retrieve the $\delta^{18}\text{O}$ value of the water in which carbonates precipitated out of equilibrium for both
280 $\delta^{18}\text{O}_{\text{carbonate}}$ and Δ_{47} .

281 In order to evaluate the applicability of such an approach to other types of carbonates, Fig. 4
282 compiles disequilibrium paired $\delta^{18}\text{O}_{\text{carbonate}}$ and Δ_{47} data from two previously published experimental
283 studies (Tang et al., 2014; Staudigel et al., 2018). These studies were chosen to further evaluate the
284 relevancy of our $\delta^{18}\text{O}_{\text{carbonate}} - \Delta_{47}$ correlation because they are the only published dataset reporting full
285 sets of *measured* $\delta^{18}\text{O}_{\text{water}}$, $\delta^{18}\text{O}_{\text{carbonate}}$ and Δ_{47} values, together with precipitation temperatures. A
286 perfect knowledge (*i.e.* measurements and not estimates) of these four parameters is mandatory here to
287 adequately test whether the use of our new $\delta^{18}\text{O}_{\text{water}}$ proxy could be generalized to a large diversity of
288 carbonates. This thus precludes plotting in Fig.4 most published Δ_{47} studies on both natural and
289 experimental samples, in which $\delta^{18}\text{O}_{\text{water}}$ and/or temperature were not directly measured. These two
290 datasets are also recent enough to allow the conversion of their Δ_{47} values to the currently used
291 normalization method (*i.e.* the CDES absolute reference frame). It will then allow comparison with
292 future studies, if measuring and reporting all these four parameters together become the rule rather than
293 the exception in Δ_{47} studies. Fig. 4a shows paired $\delta^{18}\text{O}_{\text{carbonate}}$ and Δ_{47} values of abiotic carbonates
294 produced at 5, 25 and 40°C that are known to be affected by KIF due to fast precipitation and for at least
295 two of them by KIF due to CO_2 hydration/hydroxylation prior to precipitation (Tang et al., 2004). Except
296 for these two carbonate samples, the data align on a Δ_{47} versus $\delta^{18}\text{O}_{\text{carbonate}}$ covariation curve that cannot
297 be explained by sole temperature variation. As for our microbial carbonates obtained with or without



298 CA, the average calculated $\delta^{18}\text{O}_{\text{water}}$ (Eq. 2; $-11.2 \pm 1.5\%$) matches within error with the measured
299 $\delta^{18}\text{O}_{\text{water}}$ ($-9.6 \pm 0.2\%$) (Dietzel et al., 2009).

300 Fig. 4b shows paired $\delta^{18}\text{O}_{\text{carbonate}}$ and Δ_{47} values of abiotic carbonates that were precipitated
301 during an initial CO_2 degassing + equilibration phase followed by solely equilibration with water at 5,
302 15 and 25°C (Staudigel et al., 2018). During the latter equilibration phase, even though the carbonates
303 precipitated out of isotopic equilibrium, the paired $\delta^{18}\text{O}_{\text{carbonate}}$ and Δ_{47} values align on a covariation
304 curve of average calculated $\delta^{18}\text{O}_{\text{water}}$ value (Eq. 2; $-3.0 \pm 1.1\%$) close to the measured $\delta^{18}\text{O}_{\text{water}}$ (-0.65%).
305 As a major outcome of this study, we thus anticipate that reliable $\delta^{18}\text{O}_{\text{water}}$ values of precipitation water
306 can be retrieved from carbonates presenting Δ_{47} and $\delta^{18}\text{O}_{\text{carbonate}}$ values in strong disequilibrium.

307 Some data presented in Fig. 4 also permit to evaluate the conditions of applicability of our
308 approach. In Fig. 4a, the two data points deviating from the Δ_{47} versus $\delta^{18}\text{O}_{\text{carbonate}}$ covariation curve
309 correspond to carbonates precipitated at $\text{pH} \sim 10$ and 5°C (while the others formed at pH and
310 temperatures ranging from 8.3 to 9 and 5 to 40°C , respectively) that have recorded a KIF due to CO_2
311 hydration/hydroxylation prior to precipitation (Tang et al., 2014). At $\text{pH}=10$, CO_2 reacts at 95% with
312 OH^- and at 5°C , DIC isotopic equilibration with water takes days. To a lesser extent, the KIF induced by
313 CO_2 hydroxylation seems also visible at $\text{pH}=9$ (and 40°C) where CO_2 reacts at 82% with OH^- but DIC
314 isotopic equilibration with water at 40°C only takes about 15 hours. As previously detailed, the direction
315 of these isotopic offsets from equilibrium is compatible with ab initio calculations (Guo, Ms, 2009) and
316 can be intuitively understood as follows: in carbonates derived from CO_2 hydroxylation, the $R^X_{\text{stochastic}}$
317 term used for the Δ_{47} calculation (Eq. 1) should be strongly modified as the ^{18}O concentration in OH^- and
318 H_2O is lower than in CO_2 and the reaction does not add more ^{13}C than what is present in CO_2 . This
319 might explain why in the case of disequilibria acquired through CO_2 hydroxylation, the correlation
320 between paired $\delta^{18}\text{O}$ and Δ_{47} disequilibria and the precipitation water $\delta^{18}\text{O}$ is not preserved and $\delta^{18}\text{O}_{\text{water}}$



321 cannot be reconstructed by the approach proposed here. The negative slope associated with this KIF on
322 the Δ_{47} and $\delta^{18}\text{O}_{\text{carbonate}}$ diagram (Fig. 4a) is nevertheless a good tool to identify CO_2 hydroxylation
323 reactions.

324 In Fig. 4b, during the CO_2 degassing phase of the precipitation experiment (Staudigel et al.,
325 2018), the data also deviate from the $\delta^{18}\text{O}$ versus Δ_{47} covariation curve. This behavior was interpreted by
326 the authors as a decoupling between Δ_{47} and $\delta^{18}\text{O}_{\text{carbonate}}$ values due to variable kinetics of ^{12}C -O and
327 ^{13}C -O bonding. A known difference in equilibration kinetics takes place between C and O isotopes in
328 the carbonate system as carbon isotopes equilibrate in seconds, while oxygen isotopes necessitate
329 minutes to hour to equilibrate among the different oxygen-bearing species (*i.e.* CO_2 , HCO_3^- , CO_3^{2-} , H_2O ,
330 OH^-), depending on the pH, temperature and salinity of the solution (Zeebe and Wolf-Gladrow, 2001).
331 However, note that in that experiment, the carbon isotope compositions evolved for several hours as a
332 result of CO_2 degassing (Staudigel et al., 2018). We propose here that CO_2 degassing, because it affects
333 both C and O isotopes, modifies the $R^X_{\text{stochastic}}$ term (in Eq. 1), thus preventing Δ_{47} and $\delta^{18}\text{O}$ to vary with
334 the proportionality that allows to retrieve the $\delta^{18}\text{O}_{\text{water}}$ value on a Δ_{47} versus $\delta^{18}\text{O}$ covariation plot.
335 Hence, as for CO_2 hydroxylation, in case of a KIF induced by CO_2 degassing, $\delta^{18}\text{O}_{\text{water}}$ cannot be
336 reconstructed exclusively from disequilibrium $\delta^{18}\text{O}_{\text{carbonate}}$ and Δ_{47} values.

337 In summary, we conclude that mechanisms that can drastically change the $R^X_{\text{stochastic}}$ term in Δ_{47}
338 calculation (such as CO_2 hydroxylation and degassing) prevent $\delta^{18}\text{O}_{\text{water}}$ reconstructions from paired
339 disequilibrium Δ_{47} and $\delta^{18}\text{O}_{\text{carbonate}}$ values. Nevertheless, these mechanisms lead to peculiar types of
340 carbonates (*i.e.* speleothems that form in caves for CO_2 degassing, and travertine that form on lands
341 where fluids and gas escape from subsurface reservoirs for CO_2 hydroxylation) that represent only a
342 small fraction of all the carbonates existing on Earth. We hypothesize that ureolysis, which consists in
343 two successive steps of urea hydrolysis, an exchange reaction with the H_2O molecule from the aqueous



344 medium, might give a DIC whose $R_{stochastic}^X$ term in Δ_{47} calculation is already close to that of a DIC
345 under equilibration with the $\delta^{18}\text{O}_{\text{water}}$. This would explain why even our most extreme out of equilibrium
346 carbonates still fall close to the Δ_{47} versus $\delta^{18}\text{O}_{\text{carbonate}}$ covariation line corresponding to the real $\delta^{18}\text{O}_{\text{water}}$
347 value.

348

349 **3.5 Toward a better understanding of body water $\delta^{18}\text{O}$ in biomineralizing organisms**

350 The ability to reconstruct precipitation water $\delta^{18}\text{O}_{\text{water}}$ from disequilibrium Δ_{47} and $\delta^{18}\text{O}_{\text{carbonate}}$ values
351 further allows to examine the origin of the vital effect observed in organisms for which (i) CO_2
352 degassing and hydration/hydroxylation KIF can be ruled out, and (ii) only small $\delta^{13}\text{C}$ variations are
353 observed, thus preserving the $R_{stochastic}^X$ term in Δ_{47} calculation. We hypothesize that such an approach
354 could open perspectives to understand how Δ_{47} and $\delta^{18}\text{O}$ signals are affected by kinetic effects in most of
355 the biogenic carbonates, provided that CO_2 hydroxylation or degassing do not occur prior to carbonate
356 precipitation. This approach could thus be applied to the vast majority of sedimentary carbonates
357 (Milliman et al., 1993) and since deep time (*i.e.* microbialites, brachiopods, bryozoans, bivalves,
358 foraminifera, coccoliths), even when $\delta^{18}\text{O}_{\text{carbonate}}$ variations occur in the shell of the organism.
359 Additionally, the data presented here stand as an experimental demonstration that the mechanisms
360 controlling carbonate $\delta^{18}\text{O}$ equilibration with water (*i.e.* DIC equilibration with water) also control solid
361 carbonate Δ_{47} equilibrium (Watkins et al., 2015). This result can be used to recover information on
362 biomineralization mechanisms. For example, in recent coccolithophorid *Emiliana huxleyi* culture
363 experiments, the calcitic shell produced by the organism systematically yields a 2‰ positive $\delta^{18}\text{O}$ offset
364 from equilibrium values while their Δ_{47} values seem to faithfully record precipitation temperature (Katz
365 et al., 2017). These coccolithophorids were grown in waters with different $\delta^{18}\text{O}_{\text{water}}$ compositions (*i.e.*
366 measured at -6.14, -5.82 and 0.65‰ VSMOW, that are respectively seawater A, B and C in Fig. 4c).



367 Based on our results, which demonstrate that no $\delta^{18}\text{O}$ disequilibrium should be recorded in solid
368 carbonates if the associated Δ_{47} is at equilibrium, we can assume that the coccoliths precipitated at
369 oxygen-isotope equilibrium and calculate from Eq. 2 the actual $\delta^{18}\text{O}$ value of the water in which
370 precipitation took place (respectively shifted by $1.0\pm 0.2\text{‰}$, $2.1\pm 0.4\text{‰}$ and $1.1\pm 0.7\text{‰}$ towards more
371 positive values compared to the $\delta^{18}\text{O}_{\text{water}}$ value measured for the culture medium water; Fig. 4c). This
372 could reflect a biologically-driven difference between the $\delta^{18}\text{O}$ of body water at the precipitation site
373 inside *E. huxleyi* and the $\delta^{18}\text{O}$ of ambient water (*i.e.* the culture medium water). This hypothesis is
374 supported by what is known about intracellular precipitation of coccolith performed by
375 coccolithophorids: each coccolith forms from the accumulation of coccolithosomes, which are vesicles
376 containing up to a dozen of 7 nm spherical calcium-rich granular units (Outka and Williams, 1971).
377 Water in these ~100 nm vesicles can be considered as a finite reservoir whose isotopic composition
378 could be modified through isotopic exchange with a DIC affected by metabolic isotope fractionation.
379 Another mechanism that could increase the $\delta^{18}\text{O}$ value of a finite water reservoir by equilibrating it with
380 a comparable reservoir of DIC would be the introduction of DIC systematically as CO_2 . As HCO_3^- and
381 CO_3^{2-} are enriched in ^{16}O in comparison to CO_2 , the CO_2 conversion to HCO_3^- and CO_3^{2-} at equilibrium
382 before precipitation would pump ^{16}O from water.

383 In both case scenarios, a local change in water isotopic composition requires that the water
384 molecules turnover (*i.e.* external inputs) in these cellular organites is slow enough. Coccolithosomes are
385 subunits of the Golgi complex, which is a system of flat stacked vesicles concentrating a lot of
386 membranes in a small location (Outka and Williams, 1971). It is thus plausible that in a single celled
387 organism, living in seawater and performing intracellular biomineralization, specific osmolarity and
388 water circulation regulation mechanism are occurring. It is particularly plausible in the Golgi complex,
389 whose water content is isolated from seawater by several membranes. We thus suggest that inside



390 coccolithosomes, coccoliths precursors precipitate in equilibrium with the body water for oxygen
391 isotopes, but that the body water has a different $\delta^{18}\text{O}$ value than the seawater, which explains the
392 observed $\delta^{18}\text{O}$ apparent fractionation while their Δ_{47} composition reflects culture temperature (Katz et
393 al., 2017). It has already been highlighted through geochemical analysis of coccoliths, that
394 coccolithosomes water has altered pH (Liu et al., 2018) and ion concentrations (Hermoso et al., 2017) in
395 comparison to seawater. We hypothesize that the internal $\delta^{18}\text{O}$ water would thus be another parameter
396 controlled by the coccolithophore algae.

397

398 **3.6 Ubiquity of the observed $\delta^{18}\text{O}_{\text{carbonate}} - \delta^{18}\text{O}_{\text{water}} - \Delta_{47}$ -temperature covariations in both** 399 **equilibrium and disequilibrium carbonates**

400 As shown above, in a Δ_{47} versus $\delta^{18}\text{O}_{\text{carbonate}}$ diagram, disequilibrium carbonates precipitated at fixed
401 temperature plot on the theoretical line of equilibrium carbonates precipitated with a similar $\delta^{18}\text{O}_{\text{water}}$ but
402 at a different temperature. This is illustrated in Fig. 5 where the three disequilibrium data series studied
403 in this paper (Fig. 3 for this study and Figs. 4a and b for datasets from Tang et al., (2014) and Staudigel
404 et al., (2018)) align with equilibrium data series. In other words, the values of the disequilibrium
405 $1000\ln\alpha_{\text{carbonate-water}}$ for oxygen isotopes (with $\alpha = \frac{\delta^{18}\text{O}_{\text{carbonate}}+1000}{\delta^{18}\text{O}_{\text{water}}+1000}$) are similar to the equilibrium
406 $1000\ln\alpha_{\text{carbonate-water}}$ for any given, and independently determined, apparent Δ_{47} temperature (Fig. 5). In
407 details, our closest to equilibrium data recording low apparent temperatures match better the predicted
408 equations from Coplen, (2007) and Watkins et al.,(2013), recently updated (Daëron et al., 2019). This
409 latter calibration is based on carbonates from two caves where calcite precipitate extremely slowly and is
410 thus assumed to have precipitated at equilibrium. Note that the use of these two cave samples for
411 determining the dependence to temperature of the equilibrium $1000\ln\alpha_{\text{carbonate-water}}$ relies on the



412 assumption that constant environmental conditions, including temperature in the two caves (7.9 and
413 33.7°C) and the $\delta^{18}\text{O}_{\text{water}}$ value of the precipitation water, prevailed over the whole period of carbonate
414 precipitation (Coplen, 2007; Kluge et al., 2014). In Fig. 5, the disequilibrium data recording high
415 apparent temperatures (above 100°C) match better the predicted equation of Kim and O'Neil, (1997).
416 This $1000\ln\alpha_{\text{carbonate-water}}$ dependence to temperature was established on carbonates precipitated in the
417 laboratory at well-known $\delta^{18}\text{O}_{\text{water}}$ and temperatures (from 10 to 40°C), but suspected to present a small
418 KIF due to a high precipitation rate that lowers the value of the $1000\ln\alpha_{\text{carbonate-water}}$ (Watkins et al.,
419 2013). Despite this, we used this equation to retrieve the $\delta^{18}\text{O}_{\text{water}}$ from our experimental carbonates,
420 because most of them are associated with high apparent Δ_{47} temperatures. Coplen, (2007) or Watkins et
421 al., (2013) equations would have return 2‰ lower values (ca. $-10\pm 2\%$ compared to $-8\pm 3\%$ calculated
422 with Kim and O'Neil (1997) equation). This shows how crucial it is to improve knowledge on the
423 equilibrium $1000\ln\alpha_{\text{carbonate-water}}$ at high temperatures in order to improve the accuracy and precision of
424 our new proxy for reconstructing the $\delta^{18}\text{O}_{\text{water}}$ from which carbonates, even disequilibrium ones,
425 precipitated.

426 Importantly, we here establish a new method to determine the equilibrium $1000\ln\alpha_{\text{carbonate-water}}$,
427 which consists in using the kinetics of Δ_{47} and $\delta^{18}\text{O}$ covariations during (dis)equilibration. Notably,
428 because of the very large range of apparent temperatures recorded by disequilibrium carbonates
429 (between ~40 and 200°C; Fig. 5) this method could be particularly adapted to calibrate $1000\ln\alpha_{\text{carbonate-}}$
430 water at high temperatures for which the differences between the two most popular $1000\ln\alpha_{\text{carbonate-water}}$
431 dependence to temperature equations (Kim and O'Neil, 1997; Coplen, 2007) appear larger (Fig. 5).
432 Unfortunately, none of the three experimental setups having produced these disequilibrium carbonates
433 (this study, as well as Tang et al., 2014 and Staudigel et al., 2018) were designed for the purpose of
434 calibrating the equilibrium $1000\ln\alpha_{\text{carbonate-water}}$. It is thus not possible using these datasets to propose a



435 meaningful calibration. At least in our experiment, too many phenomena including the relatively high
436 precipitation rate, variations in $\delta^{13}\text{C}$ values ($\sim 3\%$) (Thaler et al., 2017), and the presence of traces of
437 aragonite and vaterite in our carbonates (Supplementary Information) lower the accuracy of the
438 reconstructed equilibrium $1000\ln\alpha_{\text{carbonate-water}}$ values.

439 As a broader perspective, we anticipate that such an approach will help in determining critical
440 equilibrium fractionation factors for other gaseous isotopic systems (such as isotopologues of molecules
441 containing S-O bounds) or minerals of prime interest in biology and geology if clumped isotopes
442 measurements expand further beyond gaseous mass spectrometry (*e.g.* bounding between Fe-O, Fe-S,
443 Ca-C).

444

445 **4. Conclusions**

446 Our experimental results show that the information held in disequilibrium (and apparent disequilibrium)
447 carbonates is diverse and promising. First, a paired Δ_{47} and $\delta^{18}\text{O}_{\text{carbonate}}$ disequilibrium indicates that
448 carbonates have precipitated in a dynamic environment where DIC and water did not reach isotopic
449 equilibrium. In our microbial carbonate experiments, all the DIC is produced in isotopic disequilibrium
450 with water and precipitates rapidly. Accordingly, the disequilibrium O isotope compositions recorded in
451 those carbonates are maximized compared to what can be expected in nature where newly produced DIC
452 is expected to be mixed with at least partly equilibrated ambient DIC before carbonates precipitate.

453 Second, the combined use of clumped and traditional oxygen isotopic compositions allows retrieving the
454 $\delta^{18}\text{O}$ of the precipitation water, *i.e.* organism body water or environmental water, even for carbonates
455 presenting $\delta^{18}\text{O}$ and/or Δ_{47} disequilibria or apparent disequilibria. Hence, except in the case of processes
456 such as CO_2 degassing and CO_2 hydration/hydroxylation, which likely modify the $R^X_{\text{stochastic}}$ term in Δ_{47}
457 calculation, paired Δ_{47} and $\delta^{18}\text{O}_{\text{carbonates}}$ disequilibria in carbonates can be used to reconstruct the



458 oxygen-isotope composition of both DIC and water at the precipitation loci even when precipitation
459 occurred under disequilibrium conditions. Third, the (dis)equilibration trend in a Δ_{47} versus $\delta^{18}\text{O}_{\text{carbonates}}$
460 covariation diagram can be used as a new method to determine the equilibrium fractionation factor
461 between carbonate and water for a wide range of temperatures. Altogether, this open up new avenues to
462 better constrain not only past climate changes through improved paleoenvironmental reconstructions but
463 also the physiology and habitat of sea-life sensitive to ocean acidification.

464

465 **Data availability.** All the data generated and analyzed in this study are available within the paper and in
466 its Supplementary Information.

467

468 **Author contributions**

469 C.T. and A.K. conceived the research. C.T. performed the microbial precipitation experiment and the
470 $\delta^{13}\text{C}$ and $\delta^{18}\text{O}$ analyses during her PhD thesis under M.A. and B.M. supervision. A.K. performed the Δ_{47}
471 analyses during her PhD thesis under M.B. supervision. C.T. took the lead in the interpretation of the
472 results and the writing of the original draft. All authors provided critical feedback and helped shaping
473 the research, analyses and manuscript.

474

475 **Competing interests** The authors declare no competing financial interests.

476

477 **Acknowledgements**

478 This research was supported by French MRT PhD fellowships to C.T. and A.K., the Centre de
479 Recherches sur le Stockage Géologique du CO_2 (IPGP-TOTAL-Schlumberger-ADEME) (B.M. and



480 M.A.) and an Emergence grant from the Paris council to M.B. This study contributes to the IdEx
481 Université de Paris ANR-18-IDEX-0001.

482

483 **References**

484 Affek, P. A., Bar-Matthews, M., Ayalon, A., Matthews, A. & Eiler, J. M.: Glacial/interglacial
485 temperature variations in Soreq cave speleothems as recorded by “clumped isotope” thermometry.
486 *Geochim. Cosmochim. Acta* **72**, 5351–5360, <https://doi.org/10.1016/j.gca.2008.06.031>, 2008.

487 Affek, H. P.: Clumped isotopic equilibrium and the rate of isotope exchange between CO₂ and
488 water. *Am. J. Sci.* **313**, 309–325, doi: 10.2475/04.2013.02, 2013.

489 Affek, H. P. Matthews, A., Ayalon, A., Bar-Matthews, M., Burstyn, Y., Zaarur, S., & Zilberman, T.:
490 Accounting for kinetic isotope effects in Soreq Cave (Israel) speleothems. *Geochim. Cosmochim.*
491 *Acta* **143**, 303–318, <https://doi.org/10.1016/j.gca.2014.08.008>, 2014.

492 Affek, H. P. & Zaarur, S.: Kinetic isotope effect in CO₂ degassing: Insight from clumped and oxygen
493 isotopes in laboratory precipitation experiments. *Geochim. Cosmochim. Acta* **143**, 319–330,
494 <https://doi.org/10.1016/j.gca.2014.08.005>, 2014.

495 Bajnai, D., Fiebig, J., Tomašových, A., Garcia, S. M., Rollion-Bard, C., Raddatz, J., Löffler, N., Primo-
496 Ramos, C. & Brand, U.: Assessing kinetic fractionation in brachiopod calcite using clumped
497 isotopes. *Sci. Rep.* **8**, 533, <https://doi.org/10.1038/s41598-017-17353-7>, 2018.

498 Beck, W. C., Grossman, E. L. & Morse, J. W.: Experimental studies of oxygen isotope fractionation in
499 the carbonic acid system at 15, 25, and 40 °C. *Geochim. Cosmochim. Acta* **69**, 3493–3503,
500 <https://doi.org/10.1016/j.gca.2005.02.003>, 2005.

501 Bonifacie, M. Calmels, D., Eiler, J. M., Horita, J., Chaduteau, C., Vasconcelos, C., Agrinier, P., Katz,
502 A., Passey, B. H., Ferry, J. M., & Bourrand, J. J.: Calibration of the dolomite clumped isotope



- 503 thermometer from 25 to 350° C, and implications for a universal calibration for all (Ca, Mg, Fe)CO₃
504 carbonates. *Geochim. Cosmochim. Acta* **200**, 255–279, <https://doi.org/10.1016/j.gca.2016.11.028>,
505 2017.
- 506 Brand, W. A., Assonov, S. S. & Coplen, T. B.: Correction for the ¹⁷O interference in δ¹³C measurements
507 when analyzing CO₂ with stable isotope mass spectrometry (IUPAC Technical Report). *Pure Appl.*
508 *Chem.* **82**, 1719–1733, <https://doi.org/10.1351/PAC-REP-09-01-05>, 2010.
- 509 Burgener, L. K., Huntington, K. W., Sletten, R., Watkins, J. M., Quade, J., & Hallet, B.: Clumped
510 isotope constraints on equilibrium carbonate formation and kinetic isotope effects in freezing
511 soils. *Geochim. Cosmochim. Acta* **235**, 402–430, <https://doi.org/10.1016/j.gca.2018.06.006>, 2018.
- 512 Clark, I. D., Fontes, J. C. & Fritz, P.: Stable isotope disequilibria in travertine from high pH waters:
513 laboratory investigations and field observations from Oman. *Geochim. Cosmochim. Acta* **56**, 2041–
514 2050, [https://doi.org/10.1016/0016-7037\(92\)90328-G](https://doi.org/10.1016/0016-7037(92)90328-G), 1992.
- 515 Clog, M., Stolper, D. & Eiler, J. M.: Kinetics of CO₂ (g)–H₂O (l) isotopic exchange, including mass 47
516 isotopologues. *Chem. Geol.* **395**, 1–10, <https://doi.org/10.1016/j.chemgeo.2014.11.023>, 2015.
- 517 Coplen, T. B.: Calibration of the calcite–water oxygen-isotope geothermometer at Devils Hole, Nevada,
518 a natural laboratory. *Geochim. Cosmochim. Acta* **71**, 3948–3957,
519 <https://doi.org/10.1016/j.gca.2007.05.028>, 2007.
- 520 Daéron, M., Blamart, D., Peral, M. & Affek, H. P.: Absolute isotopic abundance ratios and the accuracy
521 of Δ₄₇ measurements. *Chem. Geol.* **442**, 83–96, <https://doi.org/10.1016/j.chemgeo.2016.08.014>,
522 2016.
- 523 Daéron, M., Drysdale, R. N., Peral, M., Huyghe, D., Blamart, D., Coplen, T. B., Lartaud, F. &
524 Zanchetta, G.: Most Earth-surface calcites precipitate out of isotopic equilibrium. *Nat. Commun.* **10**,
525 429, <https://doi.org/10.1038/s41467-019-08336-5>, 2019.



- 526 Dennis, K. J., Affek, H. P. & Schrag, D.: Defining an absolute reference frame for ‘clumped’ isotope
527 studies of CO₂. *Geochim. Cosmochim. Acta* **75**, 7117–7131,
528 <https://doi.org/10.1016/j.gca.2011.09.025>, 2011.
- 529 Dietzel, M., Tang, J., Leis, A. & Köhler, S. J.: Oxygen isotopic fractionation during inorganic calcite
530 precipitation—Effects of temperature, precipitation rate and pH. *Chem. Geol.* **268**, 107–115 ,
531 <https://doi.org/10.1016/j.chemgeo.2009.07.015>, 2009.
- 532 Eiler, J. M.: Paleoclimate reconstruction using carbonate clumped isotope thermometry. *Quat. Sci.*
533 *Rev.* **30**, 3575–3588, <https://doi.org/10.1016/j.quascirev.2011.09.001>, 2011.
- 534 Falk, E. S., Guo, W., Paukert, A. N., Matter, J. M., Mervine, E. M. & Kelemen, P. B.: Controls on the
535 stable isotope compositions of travertine from hyperalkaline springs in Oman: Insights from
536 clumped isotope measurements. *Geochim. Cosmochim. Acta* **192**, 1–28,
537 <https://doi.org/10.1016/j.gca.2016.06.026>, 2016.
- 538 Ghosh, P., Adkins, J., Affek H., Balta B., Guo W., Schauble E., Schrag D., & Eiler J.: ¹³C–¹⁸O bonds in
539 carbonate minerals: a new kind of paleothermometer. *Geochim. Cosmochim. Acta* **70**, 1439–1456,
540 <https://doi.org/10.1016/j.gca.2005.11.014>, 2006.
- 541 Green, M. & Taube, H.: Isotopic fractionation in the OH–H₂O exchange reaction. *J. Phys. Chem.* **67**,
542 1565–1566, <https://doi.org/10.1021/j100801a507>, 1963.
- 543 Guo, W. Carbonate clumped isotope thermometry: application to carbonaceous chondrites and effects of
544 kinetic isotope fractionation. Ph. D. thesis, California Institute of Technology, 261 p. (2009).
- 545 Guo, W., Mosenfelder, J. L., Goddard, W. A. III & Eiler, J. M.: Isotopic fractionations associated with
546 phosphoric acid digestion of carbonate minerals: insights from first principles theoretical modeling
547 and clumped isotope measurements. *Geochim. Cosmochim. Acta* **73**, 7203–7225,
548 <https://doi.org/10.1016/j.gca.2009.05.071>, 2009.



- 549 Henkes, G. A. Passey, B. H., Grossman, E. L., Shenton, B. J., Yancey, T. E., & Pérez-Huerta, A. :
550 Temperature evolution and the oxygen isotope composition of Phanerozoic oceans from carbonate
551 clumped isotope thermometry. *Earth Planet. Sci. Lett.* **490**, 40–50,
552 <https://doi.org/10.1016/j.epsl.2018.02.001>, 2018.
- 553 Hermoso, M., Lefeuvre, B., Minoletti, F., de Raféllis, M.: Extreme strontium concentrations reveal
554 specific biomineralization pathways in certain coccolithophores with implications for the Sr/Ca
555 paleoproductivity proxy. *PLoS ONE* **12**, e0185655, <https://doi.org/10.1371/journal.pone.0185655>,
556 2017.
- 557 Katz, A., Bonifacie, M., Hermoso, M., Cartigny, P. & Calmels, D.: Laboratory-grown coccoliths exhibit
558 no vital effect in clumped isotope (Δ_{47}) composition on a range of geologically relevant
559 temperatures. *Geochim. Cosmochim. Acta* **208**, 335–353, <https://doi.org/10.1016/j.gca.2017.02.025>,
560 2017.
- 561 Kelson, J. R., Huntington, K. W., Schauer, A. J., Saenger, C. & Lechler, A. R.: Toward a universal
562 carbonate clumped isotope calibration: Diverse synthesis and preparatory methods suggest a single
563 temperature relationship. *Geochim. Cosmochim. Acta* **197**, 104–131,
564 <https://doi.org/10.1016/j.gca.2016.10.010>, 2017.
- 565 Kim, S. T. & O'Neil, J. R.: Equilibrium and nonequilibrium oxygen isotope effects in synthetic
566 carbonates. *Geochim. Cosmochim. Acta* **61**, 3461–3475, [https://doi.org/10.1016/S0016-](https://doi.org/10.1016/S0016-7037(97)00169-5)
567 [7037\(97\)00169-5](https://doi.org/10.1016/S0016-7037(97)00169-5), 1997.
- 568 Kluge, T., Affek, H. P., Dublyansky, Y. & Spötl, C.: Devils Hole paleotemperatures and implications for
569 oxygen isotope equilibrium fractionation. *Earth Planet. Sci. Lett.* **400**, 251–260,
570 <https://doi.org/10.1016/j.epsl.2014.05.047>, 2014.



- 571 Létolle, R., Gegout, P., Gaveau, B. & Moranville-Regourd, M.: Isotope fractionation of ^{18}O during
572 precipitation of carbonates at very high pH. *C. R. Acad. Sci. II* **310**, 547–552, 1990b.
- 573 Liu, Y. W., Eagle, R. A., Aciego, S. M., Gilmore, R. E. & Ries, J. B.: A coastal coccolithophore
574 maintains pH homeostasis and switches carbon sources in response to ocean acidification. *Nat.*
575 *Commun.* **9**, 2857, <https://doi.org/10.1038/s41467-018-04463-7>, 2018.
- 576 Loyd, S. J. Sample, J., Tripathi, R. E., Defliese, W. F., Brooks, K., Hovland, Torres M., Marlow, J.,
577 Hancock, L.G., Martin, R. & Lyons, T.: Methane seep carbonates yield clumped isotope signatures
578 out of equilibrium with formation temperatures. *Nat. Commun.* **7**, 12274,
579 <https://doi.org/10.1038/ncomms12274>, 2016.
- 580 Manganot, X., Bonifacie, M., Gasparri, M., Götz, A., Chaduteau, C., Ader, M., & Rouchon, V.:
581 Coupling Δ_{47} and fluid inclusion thermometry on carbonate cements to precisely reconstruct the
582 temperature, salinity and $\delta^{18}\text{O}$ of paleo-groundwater in sedimentary basins. *Chem. Geol.* **472**, 44–
583 57, <https://doi.org/10.1016/j.chemgeo.2017.10.011>, 2017.
- 584 Matsuzaki, Y. Yamada, H., Chowdhury, F. A., Higashii, T., Kazama, S., & Onoda, M.: Ab initio study
585 of CO_2 capture mechanisms in monoethanolamine aqueous solution: reaction pathways from
586 carbamate to bicarbonate. *Energy Procedia* **37**, 400–406,
587 <https://doi.org/10.1016/j.egypro.2013.05.124>, 2013.
- 588 Milliman, J. D.: Production and accumulation of calcium carbonate in the ocean: budget of a nonsteady
589 state. *Global Biogeochemical Cycles*, **7**, 927–957, <https://doi.org/10.1029/93GB02524>, 1993.
- 590 Millo, C. Dupraz, S., Ader, M., Guyot, F., Thaler, C., Foy, E., & Ménez, B.: Carbon isotope
591 fractionation during calcium carbonate precipitation induced by ureolytic bacteria. *Geochim.*
592 *Cosmochim. Acta* **98**, 107–124, <https://doi.org/10.1016/j.gca.2012.08.029>, 2012.



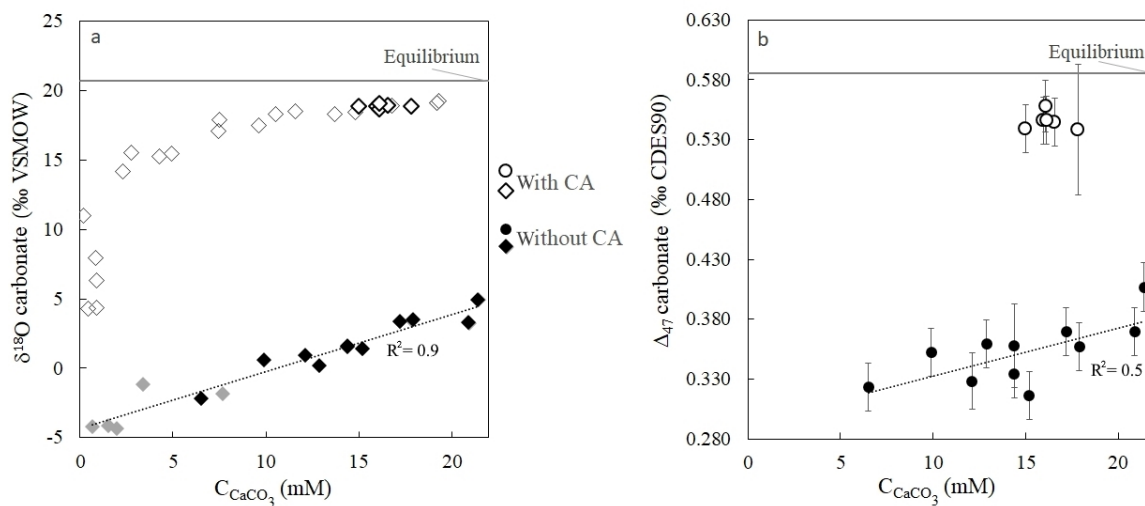
- 593 Outka, D. E., & Williams, D. C.: Sequential coccolith morphogenesis in *Hymenomonas carterae*. *J.*
594 *Protozool.* **18**, 285–297, <https://doi.org/10.1111/j.1550-7408.1971.tb03319.x>, 1971.
- 595 Rollion-Bard, C., Chaussidon, M. & France-Lanord, C.: pH control on oxygen isotopic composition of
596 symbiotic corals. *Earth Planet. Sci. Lett.* **215**, 275–288, [https://doi.org/10.1016/S0012-](https://doi.org/10.1016/S0012-821X(03)00391-1)
597 [821X\(03\)00391-1](https://doi.org/10.1016/S0012-821X(03)00391-1), 2003.
- 598 Saenger, C. Affek, H. P., Felis, T., Thiagarajan, N., Lough, J. M., & Holcomb, M.: Carbonate clumped
599 isotope variability in shallow water corals: Temperature dependence and growth-related vital
600 effects. *Geochim. Cosmochim. Acta* **99**, 224–242, <https://doi.org/10.1016/j.gca.2012.09.035>, 2012.
- 601 Spooner, P. T. Guo, W., Robinson, L. F., Thiagarajan, N., Hendry, K. R., Rosenheim, B. E., & Leng, M.
602 J.: Clumped isotope composition of cold-water corals: A role for vital effects?. *Geochim.*
603 *Cosmochim. Acta* **179**, 123–141, <https://doi.org/10.1016/j.gca.2016.01.023>, 2016.
- 604 Staudigel, P. T., & Swart, P. K.: A kinetic difference between ¹²C-and ¹³C-bound oxygen exchange rates
605 results in decoupled $\delta^{18}\text{O}$ and Δ_{47} values of equilibrating DIC solutions. *Geochem. Geophys.*
606 *Geosystems* **19**, 2371–2383, <https://doi.org/10.1029/2018GC007500>, 2018.
- 607 Tang, J., Dietzel, M., Fernandez, A., Tripathi, A. K. & Rosenheim, B. E.: Evaluation of kinetic effects on
608 clumped isotope fractionation (Δ_{47}) during inorganic calcite precipitation. *Geochim. Cosmochim.*
609 *Acta* **134**, 120–136, <https://doi.org/10.1016/j.gca.2014.03.005>, 2014.
- 610 Thaler, C. Millo, C., Ader, M., Chaduteau, C., Guyot, F., & Ménez, B.: Disequilibrium $\delta^{18}\text{O}$ values in
611 microbial carbonates as a tracer of metabolic production of dissolved inorganic carbon. *Geochim.*
612 *Cosmochim. Acta* **199**, 112–129, <https://doi.org/10.1016/j.gca.2016.10.051>, 2017.
- 613 Thiagarajan, N., Adkins, J. & Eiler, J.: Carbonate clumped isotope thermometry of deep-sea corals and
614 implications for vital effects. *Geochim. Cosmochim. Acta* **75**, 4416–4425,
615 <https://doi.org/10.1016/j.gca.2011.05.004>, 2011.



- 616 Tripathi, A. K., Hill, P. S., Eagle, R. A., Mosenfelder, J. L., Tang, J., Schauble, E. A., Eiler, J. M.,
617 Zeebe, R. E., Uchikawa, J., Coplen, T. B., Ries, J. B. & Drew, H.: Beyond temperature: Clumped
618 isotope signatures in dissolved inorganic carbon species and the influence of solution chemistry on
619 carbonate mineral composition. *Geochim. Cosmochim. Acta* **166**, 344–371,
620 <https://doi.org/10.1016/j.gca.2015.06.021>, 2015.
- 621 Urey, H. C., Lowenstam, H. A., Epstein, S. & McKinney, C.R. Measurement of paleotemperatures and
622 temperatures of the Upper Cretaceous of England, Denmark, and the south-eastern United States.
623 *Geol. Soc. Am. Bull.* **62**, 399–416, [https://doi.org/10.1130/0016-](https://doi.org/10.1130/0016-7606(1951)62[399:MOPATO]2.0.CO;2)
624 [7606\(1951\)62\[399:MOPATO\]2.0.CO;2](https://doi.org/10.1130/0016-7606(1951)62[399:MOPATO]2.0.CO;2), 1951.
- 625 Usdowski, E., Michaelis, J., Bottcher, M. E. & Hoefs, J.: Factors for the oxygen isotope equilibrium
626 fractionation between aqueous and gaseous CO₂, carbonic-acid, bicarbonate, carbonate, and water
627 (19 °C). *Z. Phys. Chem.* **170**, 237–249, 1991.
- 628 Watkins, J. M., Nielsen, L. C., Ryerson, F. J. & DePaolo, D. J.: The influence of kinetics on the oxygen
629 isotope composition of calcium carbonate. *Earth Planet. Sci. Lett.* **375**, 349–360,
630 <https://doi.org/10.1016/j.epsl.2013.05.054>, 2013.
- 631 Watkins, J. M. & Hunt, J. D.: A process-based model for non-equilibrium clumped isotope effects in
632 carbonates. *Earth Planet. Sci. Lett.* **432**, 152–165, <https://doi.org/10.1016/j.epsl.2015.09.042>, 2015.
- 633 Zeebe, R. E. & Wolf-Gladrow, D.: *CO₂ in Seawater: Equilibrium, Kinetics, Isotopes*. Elsevier
634 Oceanography Book Series, v. **65**. 346 pp. 2001

635

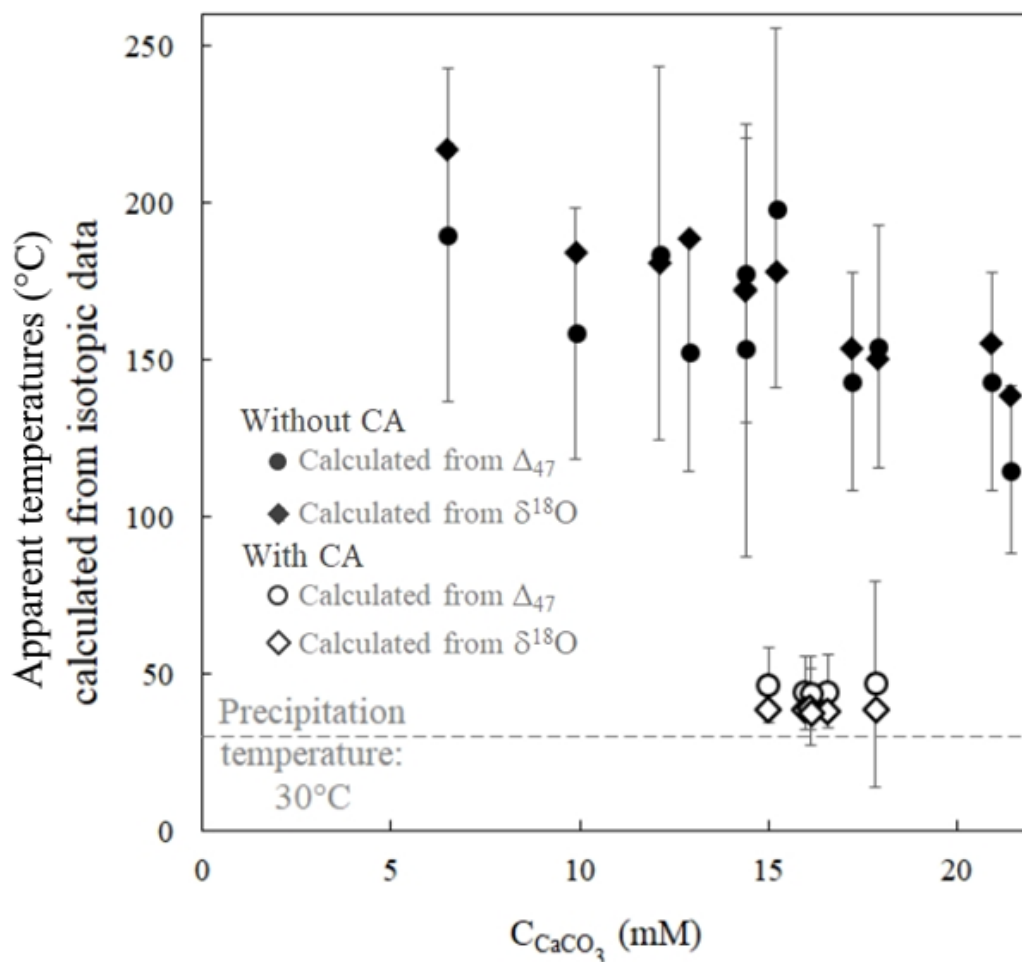
636 **Figures & Figure Legends**



637

638 **Figure 1 | Strong $\delta^{18}\text{O}$ and Δ_{47} disequilibria recorded in microbial carbonates** as shown by
639 $\delta^{18}\text{O}_{\text{carbonate}}$ (a) and Δ_{47} (b) values of calcium carbonates (CaCO_3) precipitated during bacterial ureolysis
640 at 30°C (with and without carbonic anhydrase, CA; open and solid symbols, respectively) as a function
641 of carbonate accumulation (C_{CaCO_3}). Black symbols correspond to samples for which both Δ_{47} and $\delta^{18}\text{O}$
642 measurements were performed. The grey horizontal lines are equilibrium $\delta^{18}\text{O}_{\text{carbonate}}$ and Δ_{47} values at
643 30°C for calcite following Bonifacie et al., (2017) and Kim and O'Neil, (1997) calibrations,
644 respectively. Uncertainties (one standard deviation, 1SD) are smaller than symbol for $\delta^{18}\text{O}$ and C_{CaCO_3}
645 values (Supplementary Table 1). Reported Δ_{47} uncertainties are detailed in Methods and Supplementary
646 Discussion.

647

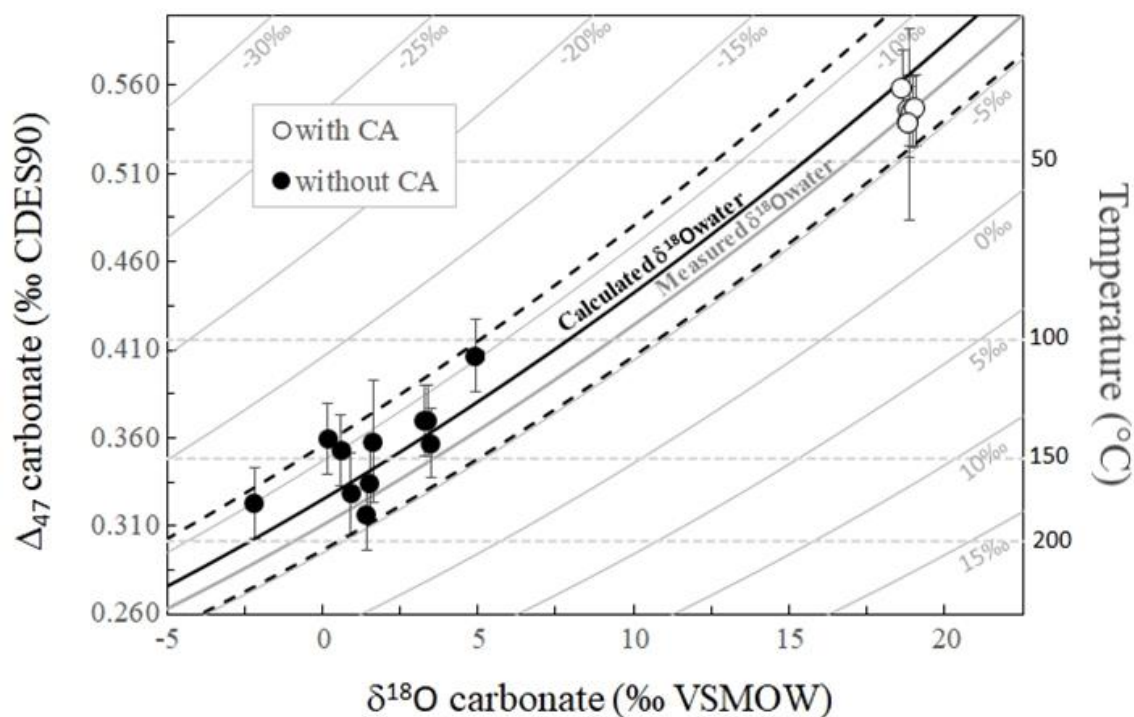


648

649 **Figure 2 | $\delta^{18}O_{\text{carbonate}}$ and Δ_{47} disequilibria in microbial carbonates induce comparable biased**
650 **estimates of precipitation temperature** as illustrated by apparent temperatures calculated from the
651 carbonate $\delta^{18}O_{\text{carbonate}}$ and Δ_{47} signatures as a function of $CaCO_3$ accumulation. Open and solid symbols
652 refer to the experiments with and without CA, respectively. The dashed grey line corresponds to the
653 actual precipitation temperature. Apparent temperatures are respectively calculated from the $\delta^{18}O_{\text{carbonate}}$
654 and Δ_{47} calibrations to temperature of Bonifacie et al., (2017) and Kim and O'Neil, (1997). Reported
655 uncertainties were calculated as the propagation of the one standard deviation (1SD) error of the isotopic
656 data in the calibration equations (Supplementary Information).



657



658

659

Figure 3 | Combined $\delta^{18}\text{O}_{\text{carbonate}}$ and Δ_{47} disequilibria of microbial carbonates precipitated at

660

30°C allow reconstruction of the $\delta^{18}\text{O}$ of the water ($\delta^{18}\text{O}_{\text{water}}$) in which they precipitate. Solid grey

661

curves represent the calculated Δ_{47} and $\delta^{18}\text{O}_{\text{carbonate}}$ compositions of carbonates precipitated at oxygen

662

isotope equilibrium from water with fixed $\delta^{18}\text{O}_{\text{water}}$ values (indicated on each curve) and variable

663

temperatures. Horizontal dashed grey lines are calculated for fixed temperatures and variable $\delta^{18}\text{O}_{\text{water}}$.

664

The average $\delta^{18}\text{O}_{\text{water}}$ value of $-6.6 \pm 0.4\text{‰}$ measured in our experiments is reported using the thick solid

665

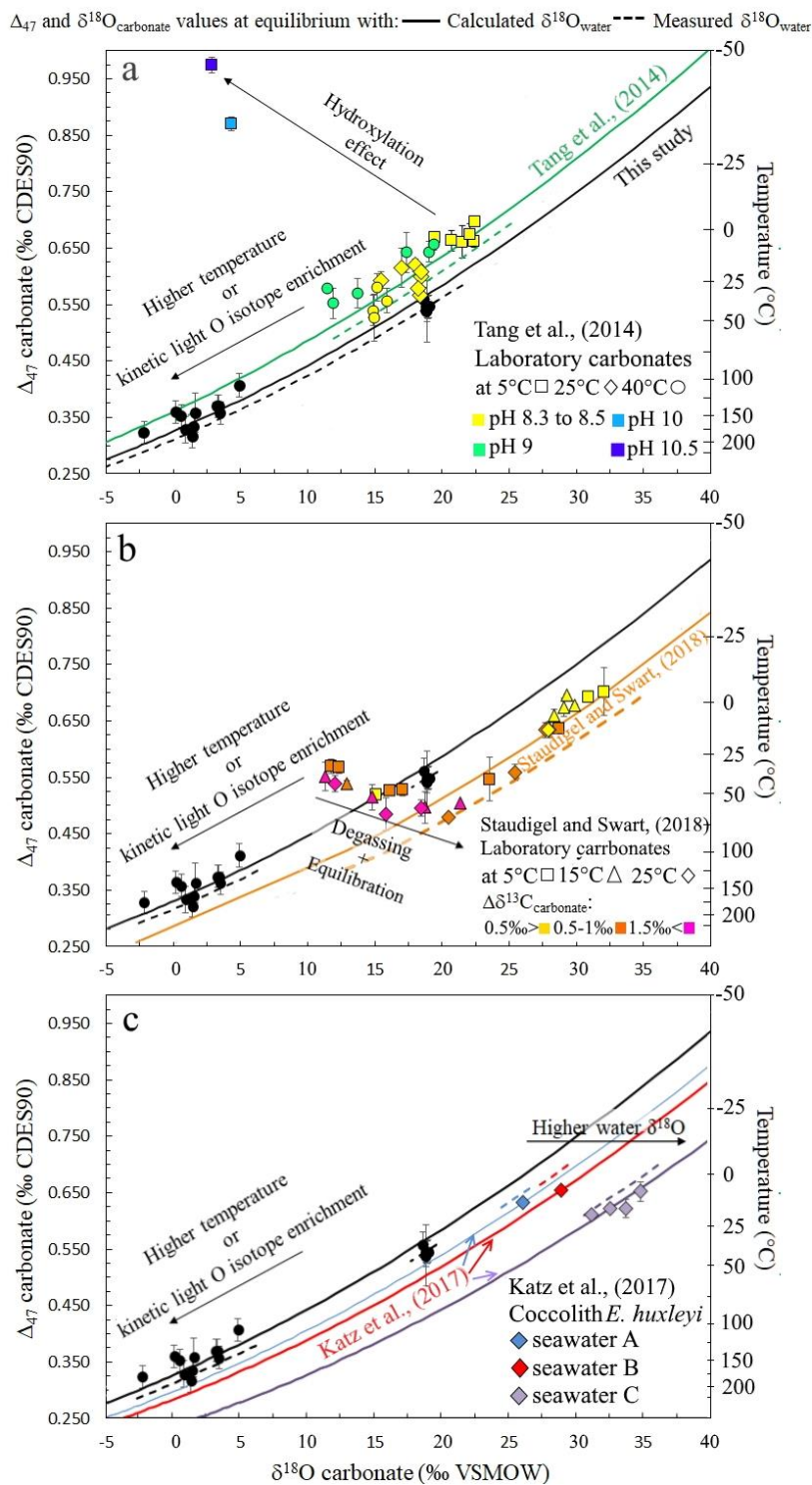
grey curve. The solid black curve was obtained using the $\delta^{18}\text{O}_{\text{water}}$ calculated with Eq. 1 ($-8.0 \pm 2.8\text{‰}$)

666

with its associated errors (dashed black curves).

667

668

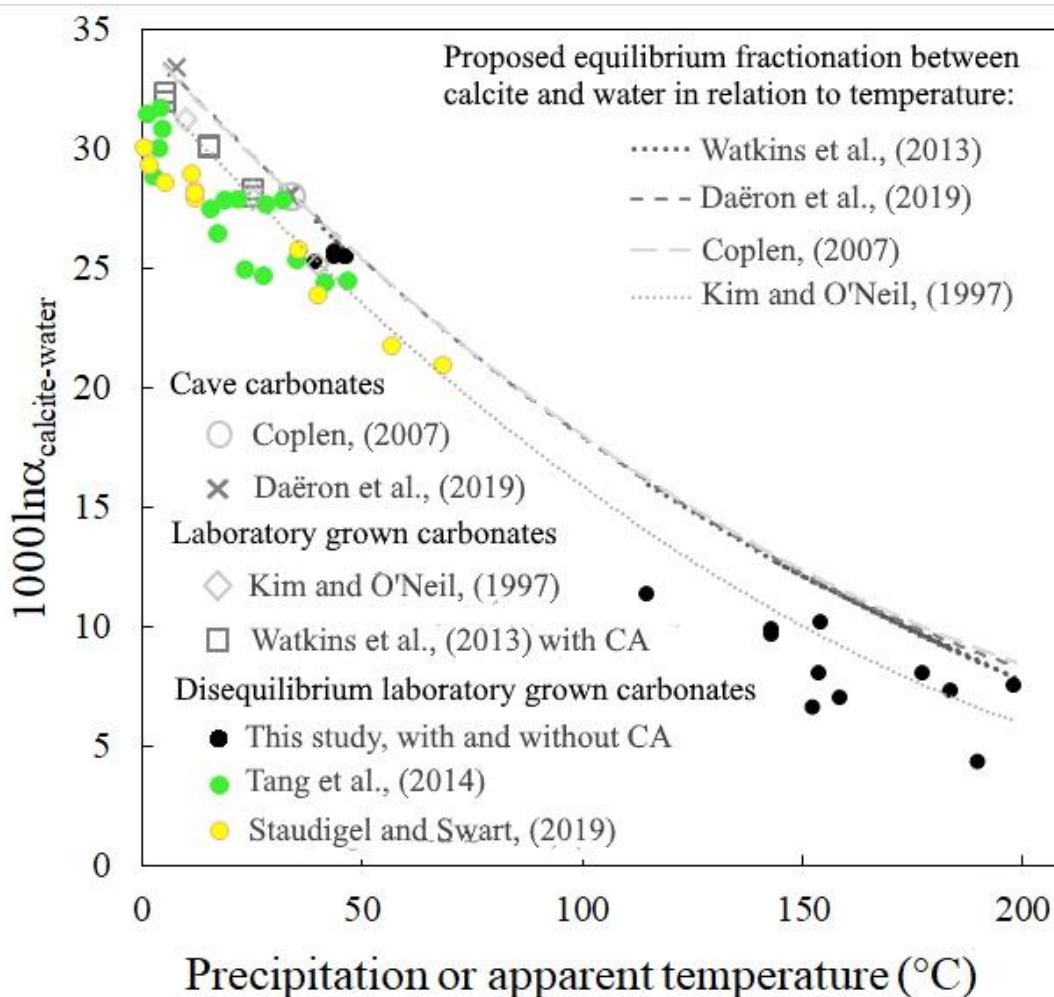




670 **Figure 4 | Δ_{47} and $\delta^{18}\text{O}_{\text{carbonate}}$ relationship to precipitation water $\delta^{18}\text{O}_{\text{water}}$ for other solid**
671 **carbonates presenting oxygen isotope disequilibria.** In (a) to (c) black data series (this study,
672 performed at 30°C) shows how kinetic oxygen isotope fractionation in the DIC prior to carbonate
673 precipitation can be mistaking for high temperature isotopic equilibrium. Similarly to Fig. 3, the solid
674 curves were obtained using the $\delta^{18}\text{O}_{\text{water}}$ calculated with Eq. 1. (a) Abiotic carbonates from Tang et al.,
675 (2014) illustrating the effect of CO_2 hydroxylation on Δ_{47} and $\delta^{18}\text{O}_{\text{carbonate}}$ values (various pH plotted
676 with different colors, various temperatures plotted with different symbols). (b) Abiotic carbonates from
677 Staudigel and Swart, (2019) illustrating the effect of CO_2 degassing and DIC oxygen isotope
678 equilibration with water on Δ_{47} and $\delta^{18}\text{O}_{\text{carbonate}}$ values. $\Delta\delta^{13}\text{C}_{\text{carbonate}}$ stands for the difference between
679 the $\delta^{13}\text{C}$ value measured in carbonates and the final $\delta^{13}\text{C}$ of the data series at the end of equilibration
680 (various $\Delta\delta^{13}\text{C}$ ranges plotted with different colors, various temperatures plotted with different
681 symbols). (c) Coccolithophorid *E. huxleyi* grown at 7, 10, 15, 20 and 25°C from Katz et al., (2017)
682 showing how coccoliths with equilibrium Δ_{47} values record the equilibrium $\delta^{18}\text{O}_{\text{water}}$ of their body water,
683 which differs from that of the culture medium (*i.e.* artificial seawaters A, B, and C plotted with different
684 colors).
685



686



687

688 **Figure 5 | The relation to temperature of equilibrium oxygen isotope fractionation factor between**
689 **calcium carbonate and water ($1000 \ln \alpha_{\text{calcite-water}}$) appears to be retrievable from solid carbonates**
690 **(mainly calcites) in strong clumped and oxygen isotope disequilibrium such as our microbial**
691 **carbonates (black dots, precipitated at 30°C) and two additional data series of laboratory grown**
692 **carbonates showing disequilibrium fractionation (Tang et al., 2014; Staudigel and Swart, 2019) (green**
693 **and yellow dots, respectively). The data points affected by CO₂ hydroxylation (Tang et al., 2014) or CO₂**
694 **degassing (Staudigel and Swart, 2019) (see Fig.4) are not included. Grey symbols correspond to cave**
695 **carbonates precipitated at or near equilibrium (Coplen, 2007; Daëron et al., 2019) or laboratory**



696 experiments (Kim and O'Neil, 1997; Watkins et al., 2013). Those grey data series are usually considered
697 as representative of the equilibrium fractionation factor between calcium carbonate and water whose
698 relations to temperature, extrapolated at high temperature, are illustrated by the different dashed curves.
699 Plotted temperatures corresponds to precipitation temperatures except for disequilibrium carbonates for
700 which apparent temperatures have been calculated based on Δ_{47} values. Errors are included in the
701 symbol size.